

Study of Staggered Magnetization in the Spin- S Square-Lattice Heisenberg Model Using Spiral Boundary Conditions

Masahiro Kadosawa^{1*}, Masaaki Nakamura², Yukinori Ohta¹, and Satoshi Nishimoto^{3,4}

¹*Department of Physics, Chiba University, Chiba 263-8522, Japan*

²*Department of Physics, Ehime University, Ehime 790-8577, Japan*

³*Department of Physics, Technical University Dresden, 01069 Dresden, Germany*

⁴*Institute for Theoretical Solid State Physics, IFW Dresden, 01171 Dresden, Germany*

We propose an efficient numerical method to obtain local order parameter in two-dimensional systems using spiral boundary conditions. As a benchmark, we first estimate the magnitude of staggered magnetization for the $S = 1/2$ XXZ Heisenberg model on a square lattice in the whole range of the XXZ anisotropy by density-matrix renormalization group technique. The validity of our method is confirmed by comparing our results with the previous analytical and numerical studies. Then, as further demonstration, we apply our method to obtain the staggered magnetization for the higher-spin cases from $S = 1$ to $S = 6$. The accuracy of the obtained results is validated using the series expansion and the spin-wave theory.

The Heisenberg model¹⁾ is used to study the magnetic properties of various materials. The geometry of spin network as well as the exchange anisotropy (Δ) are key factors to determine the magnetic ground state. Such anisotropy often exists in real materials due to the effects of crystal fields and so on.^{2,3)} While easy-axis anisotropy typically reduces quantum fluctuations, easy-plane one brings a two-dimensional (2D) system to the BKT universality class.⁴⁾ Interestingly, recent studies reported a possible tuning of Δ by magnetic field in $[\text{Cu}(\text{pz})_2(2\text{-HOpy})_2](\text{PF}_6)_2$ ⁵⁾ and a switching between $\Delta > 1$ and $\Delta < 1$ by coligands in cobalt complexes.⁶⁾ In particular, easy-plane magnets provide an exciting platform for studying topological excitations referred to as vortices.⁷⁾

Another important factor is the magnitude of spin (S). One may think that a quantum system just approaches the classical limit with increasing S . However, the actual physics is not so simple because of the presence of specific features like the Haldane state. In fact, even nowadays, fascinating experimental measurements for high- S materials have been successively reported: For example, square magnets $\text{Ba}_2\text{FeSi}_2\text{O}_7$ ($S = 2$),⁸⁻¹⁰⁾ NaMnSbO_4 ($S = 5/2$),¹¹⁾ triangular magnets PbMnTeO_6 ($S = 3/2$),¹²⁾ AgCrSe_2 ($S = 3/2$),¹³⁾ $\alpha\text{-CrOO}(\text{H,D})$ ($S = 3/2$),¹⁴⁾ $\text{Ba}_8\text{MnNb}_6\text{O}_{24}$ ($S = 5/2$),¹⁵⁾ Ag_2FeO_2 ($S = 5/2$),¹⁶⁾ honeycomb magnet CoPS_3 ($S = 3/2$),¹⁷⁾ kagome magnets $\text{Cs}_2(\text{K,Na})\text{Cr}_3\text{F}_{12}$ ($S = 3/2$),¹⁸⁾ $\text{Li}_9\text{Fe}_3(\text{P}_2\text{O}_7)_3(\text{PO}_4)_2$ ($S = 5/2$),¹⁹⁾ $\text{PbFe}_3(\text{PO}_4)(\text{SO}_4)(\text{OH})_6$ ($S = 5/2$).²⁰⁾ Furthermore, the exploration of spin-liquid ground state is recently heating up with the appearance of high- S Kitaev materials.²¹⁻²³⁾

Under these circumstances, numerical techniques to systematically study the high- S Heisenberg systems in a wide range of Δ are increasingly required. However, the computational cost would be significant for such cases, so that it is often hard to obtain quantities accurately in the thermodynamic limit. Thus, in this paper, we propose an efficient method to obtain order parameter for 2D systems with spiral boundary conditions (SBC). Using SBC, a 2D system can be exactly projected onto a one-dimensional (1D) periodic chain

with translation symmetry. This enables us to perform optimal DMRG calculations and simple finite-size scaling. As a benchmark, we estimate the magnitude of staggered magnetization for $S = 1/2$ XXZ square-lattice Heisenberg model by density-matrix renormalization group (DMRG). To confirm the validity of our method, the results are compared to the previous studies by DMRG,²⁴⁾ quantum Monte Carlo (QMC),^{25,26)} spin wave theory (SWT),²⁷⁻²⁹⁾ series expansion (SE),³⁰⁻³⁷⁾ and coupled-cluster method (CCM).³⁸⁾ We then demonstrate that this method can achieve a high performance level even for high- S cases.

The Hamiltonian of the spin- S XXZ model on a square lattice is written as $\mathcal{H} = \sum_{\langle ij \rangle} (S_i^x S_j^x + S_i^y S_j^y + \Delta S_i^z S_j^z)$, where S_i^γ ($\gamma = x, y, z$) are the spin- S operators, Δ is the anisotropy parameter, and the sum $\langle ij \rangle$ runs over all nearest-neighbor pairs. It is known that this model exhibits long-range order for any S and Δ .³⁹⁾ There are three phases depending on Δ :³⁹⁻⁴²⁾ (i) For $\Delta > 1$ easy-axis Néel phase with antiferromagnetic (AFM) spin alignment along the z -direction, (ii) for $-1 < \Delta < 1$ easy-plane Néel (XY) phase with AFM spin alignment along some arbitrary direction in the xy -plane, and (iii) for $\Delta < -1$ ferromagnetic (FM) phase with fully-polarized spins along the z -direction. The phase transitions at $\Delta = \pm 1$ are both first order. For $\Delta = -1$ this model can be exactly solved: The ground state is two-fold degenerate with energy $E_0 = -2NS^2$. One of them is expressed as $|\Psi_0(\text{XY})\rangle = \sum_m \lambda_m |\psi_m\rangle$, where $|\psi_m\rangle$ are bases restricted to $S_{\text{tot}}^z = \sum_{i=1}^L \langle S_i^z \rangle = 0$ subspace, m is summed over all possible combinations of the spin configurations, and λ_m are determined for each S (see Supplementary data⁴³⁾). The magnitude of staggered magnetization is S with the direction parallel to the xy -plane. The other is a FM state $|\Psi_0(\text{FM})\rangle = \frac{1}{\sqrt{2}}(|\uparrow\rangle + |\downarrow\rangle)$, where $|\uparrow\rangle$ and $|\downarrow\rangle$ denote fully-polarized states toward z and $-z$ directions, respectively. These states $|\Psi_0(\text{XY})\rangle$ and $|\Psi_0(\text{FM})\rangle$ are orthogonal. Also, the system is simplified to an Ising model at $\Delta \rightarrow \infty$ (Ising limit).

First, we explain our method for estimating the magnitude of magnetization. In general, it is difficult to estimate an order parameter for 2D system with DMRG because not only the implementation itself is challenging

arXiv:2211.09560v2 [cond-mat.str-el] 29 Dec 2022

*afna1728@chiba-u.jp

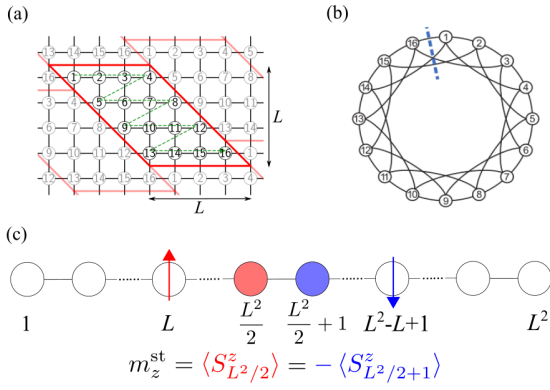


Fig. 1. (Color online) (a) 2D square lattice with $L = 4$, where the region framed by red line is the original cluster. (b) 1D representation of (a) by numbering sites along green line. An open chain is created by cutting L bonds between two sites (dotted line). (c) Schematic picture of 1D open chain used for the DMRG calculations of m_z^{st} . The arrows denote pinned spins and m_z^{st} is measured at the filled sites.

but also finite-size scaling analysis is not straightforward. We manage to resolve these issues by mapping 2D cluster onto 1D translation-symmetric chain using SBC. Here, the original 2D square lattice with $L \times L$ sites is mapped onto a 1D chain with nearest- and $(L - 1)$ -th neighbor bonds.^{44,45)} An example of this mapping scheme for a 4×4 cluster is illustrated in Fig. 1(a,b). Thus, the Hamiltonian is translated to $\mathcal{H} = \sum_{i=1}^{L^2} (S_i^x S_{i+1}^x + S_i^y S_{i+1}^y + \Delta S_i^z S_{i+1}^z) + \sum_{i=1}^{L^2} (S_i^x S_{i+(L-1)}^x + S_i^y S_{i+(L-1)}^y + \Delta S_i^z S_{i+(L-1)}^z)$. As a result, quantum entanglement is uniformly distributed over the projected 1D chain due to the translation symmetry. It is also important that the distance of the longest bonds is minimized to be $L - 1$. These conditions enable us to optimally perform DMRG calculations. In addition, since the lattice site is indexed by a single coordinate i instead of two coordinates (i, j) in 2D cluster, just one finite-size scaling analysis is required to obtain physical quantity in the thermodynamic limit.

For an Néel state an order parameter is the magnitude of staggered magnetization. Since the Néel order with $\mathbf{k} = (\pi, \pi)$ in the original 2D representation is expressed as that with $k = \pi$ along the projected 1D chain, the order parameter may be defined by retaining half-amplitude of the Friedel oscillation of $\langle S_i^\alpha \rangle$ ($\alpha = x, y, \text{ or } z$) starting from the system edges if we use an open chain. Such an open chain can be created by cutting L bonds between two sites of the projected 1D periodic chain [see Fig. 1(b)]. In practice, we measure the local moments of central spins $\langle S_{L^2/2}^z \rangle, \langle S_{L^2/2+1}^z \rangle$ ($\langle S_{L^2/2}^x \rangle, \langle S_{L^2/2+1}^x \rangle$) with pinning two spins near the system edges like $\langle S_L^z \rangle = 1/2, \langle S_{L^2-L+1}^z \rangle = -1/2$ ($\langle S_L^x \rangle = 1/2, \langle S_{L^2-L+1}^x \rangle = -1/2$) in the easy-axis (easy-plane) Néel phase. Thus, the order parameters for the easy-axis and easy-plane Néel states are defined as $m_z^{\text{st}} = |\langle S_{L^2/2}^z \rangle - \langle S_{L^2/2+1}^z \rangle|/2$ and $m_x^{\text{st}} = |\langle S_{L^2/2}^x \rangle - \langle S_{L^2/2+1}^x \rangle|/2$, respectively [see Fig. 1(c)]. Typically, such a pinning may be naively placed at system edges, i.e., at $i = 1, i = L^2$. However, since outer $L - 1$ sites for both edges lose the original bonds, the pinnings are placed at the inner sites $i = L, i = L^2 - L + 1$ to avoid an underestimate of order parameter (also see below).

We use DMRG method⁴⁶⁾ to calculate the magnitude of staggered magnetization. We study open chains with length

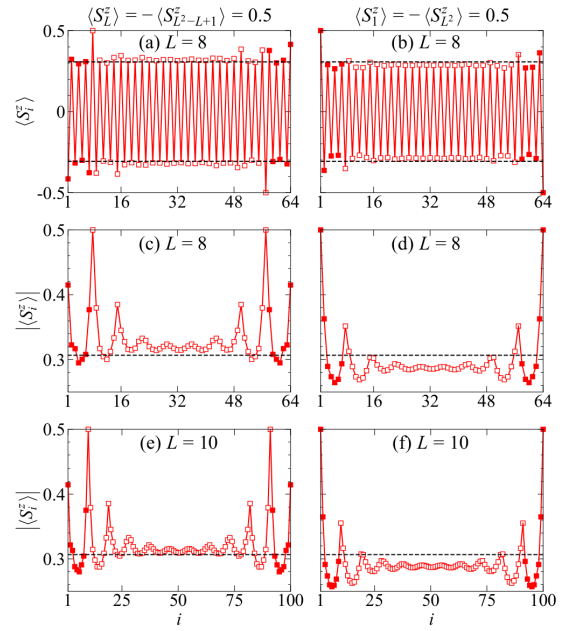


Fig. 2. (Color online) (a) Local spin moment $\langle S_i^z \rangle$ and (c,e) $|\langle S_i^z \rangle|$ with pinning at $i = L, i = L^2 - L + 1$. (b,d,f) The same quantities with pinning at $i = 1, i = L^2$. Dashed lines ($m_z^{\text{st}} = 0.3067^{24}$) are guide for the convergence. The solid squares correspond to sites which lose the original bonds (see text).

up to $N = L^2 = 196$ sites. We keep up to $\chi = 8000$ density-matrix eigenstates, and the discarded weight is on the order of 10^{-5} at most. The calculated values are extrapolated to $\chi \rightarrow \infty$ if necessary. More detailed data on the accuracy of our DMRG calculations are given in the Supplemental Material.⁴³⁾ For comparison, the performances using various boundary conditions are also shown.

As an illustration, we plot the Friedel oscillation of $\langle S_i^z \rangle$ for $S = 1/2$ and $\Delta = 1$ in Fig. 2(a), where spins at $i = L, i = L^2 - L + 1$ are pinned. A staggered oscillation with $k = \pi$ is obviously seen. Also, the oscillation of $\langle S_i^z \rangle$ seems to converge well towards the system center as shown in Fig. 2(c,e). Let us then look over what happens if the edge spins at $i = 1, i = L^2$ are pinned. The Friedel oscillation for this case is shown in Fig. 2(b). We find that the amplitude near the pinned spins is visibly smaller than that around the system center. Accordingly, the amplitude tends to be rather small for fixed L as in Fig. 2(d,f). Hence perhaps, the order parameter might be underestimated or the convergence to the thermodynamic limit could be slow. Since the outer $L - 1$ sites for each edge lose the original bond connections by cutting the projected 1D periodic chain, it is more reasonable to regard the outer $2(L - 1)$ spins in total as ‘edged-spin group’. Thus, the pinnings for the inner spins placed at $i = L, i = L^2 - L + 1$ would be a good choice.

We begin by discussing the performance of our method at $\Delta = 1$ between the easy-axis Néel and XY phases for $S = 1/2$. Since quantum fluctuations are largest and entanglement range is maximized in this case, it is rather difficult to numerically estimate the magnitude of magnetization for the thermodynamic limit. Actually, its accurate estimation had been a longstanding problem until 2010s.^{24,26)} Therefore, this is a good benchmark to evaluate our method. The direction

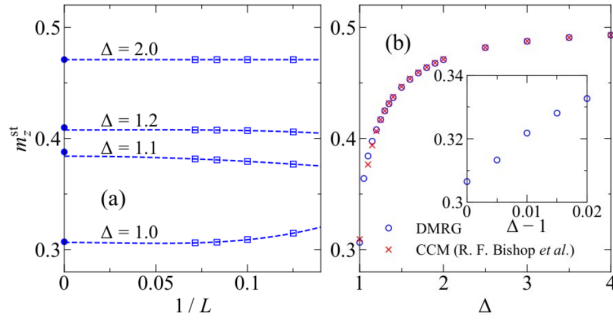


Fig. 3. (Color online) (a) Finite-size scaling analysis of m_z^{st} for $S = 1/2$ and $\Delta \geq 1$. Solid circles at $1/L = 0$ are our previous results using periodic chains.⁴⁵⁾ (b) Extrapolated values of m_z^{st} as a function of Δ . The results of CCM³⁸⁾ are shown by red crosses. The inset shows m_z^{st} as a function of $\Delta - 1$ for a narrow range near $\Delta = 1$.

Table I. Extrapolated values of m_z^{st} in the easy-axis Néel phase ($\Delta \geq 1$) for $S = 1/2$. Results obtained by DMRG and CCM methods are compared: $\delta = m_z^{\text{st}}(\text{CCM}) - m_z^{\text{st}}(\text{DMRG})$.

Δ	$m_z^{\text{st}}(\text{DMRG})$	$m_z^{\text{st}}(\text{CCM})$	δ
1.0	0.3065	0.3093	0.0028
1.2	0.4079	0.4067	-0.0012
1.5	0.4459	0.4466	0.0007
2.0	0.4709	0.4712	0.0003
3.0	0.4874	0.4875	0.0001
4.0	0.4930	0.4930	<0.0001

of magnetization is now arbitrary. So, assuming it parallel to the z -axis, we calculate m_z^{st} . In this way, we can restrict the spin configurations to a subspace with $S_z^{\text{tot}} = \sum_i S_i^z = 0$. In Fig. 3(a) we perform finite-size scaling analysis of m_z^{st} , where open chains with length up to $N = L^2 = 196$ sites are studied. The convergence of m_z^{st} with $1/L$ seems to be fast enough to perform a reliable scaling. By fitting with $m_z^{\text{st}}(L) = m_z^{\text{st}} + a/L^2 + b/L^3$, we obtain $m_z^{\text{st}} = 0.3065$, which is in good agreement with those by previous numerical estimations: DMRG ($m_z^{\text{st}} = 0.3067$),²⁴⁾ QMC ($m_z^{\text{st}} = 0.30743$),²⁶⁾ and CCM ($m_z^{\text{st}} = 0.3093$).³⁸⁾ We also note that this value is only slightly smaller than our previous estimation using periodic chains ($m_z^{\text{st}} = 0.3071 \pm 0.0005$).⁴⁵⁾

The system is gapless at $\Delta = 1$. While on the other hand, the gap opens between the $S_z^{\text{tot}} = 0$ ground state and $S_z^{\text{tot}} = 1$ excited state for $\Delta > 1$. This implies that the direction of staggered magnetization is uniquely fixed parallel to the z -axis. Let us then estimate m_z^{st} for $\Delta > 1$. Finite-size scaling analyses of m_z^{st} for some Δ values are shown in Fig. 3(a). For larger Δ the size-dependence of m_z^{st} is smaller as expected from the fact that entanglement range is reduced by the reduction of quantum fluctuations. The extrapolated values of m_z^{st} are plotted as a function of Δ in Fig. 3(b). We can see that m_z^{st} converges rapidly to the Ising value $1/2$ with Δ . For comparison, recent data from CCM method³⁸⁾ are also shown. The agreement seems to be overall good. The values of m_z^{st} are particularly compared in Table I. The deviation becomes larger with approaching $\Delta = 1$. Nevertheless, even though the uncertainties of the scaling to $L \rightarrow \infty$ in DMRG as well as of the scaling to $m \rightarrow \infty$ in the so-called LSUB _{m} level of approxi-

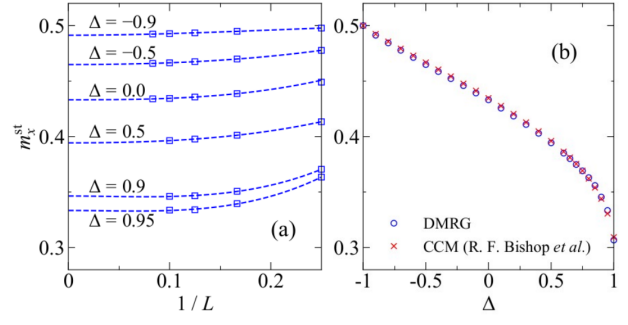


Fig. 4. (Color online) (a) Finite-size scaling analysis of m_x^{st} for $S = 1/2$ and $|\Delta| < 1$. (b) Extrapolated values of m_x^{st} as a function of Δ . The results of CCM³⁸⁾ are shown by red crosses.

Table II. Extrapolated values of m_x^{st} in the XY phase ($-1 < \Delta \leq 1$) for $S = 1/2$. Results obtained by DMRG and CCM methods are compared: $\delta = m_x^{\text{st}}(\text{CCM}) - m_x^{\text{st}}(\text{DMRG})$.

Δ	$m_x^{\text{st}}(\text{DMRG})$	$m_x^{\text{st}}(\text{CCM})$	δ
-1.0	0.5000	0.5000	0.0000
-0.8	0.4844	0.4856	0.0012
-0.5	0.4649	0.4667	0.0018
0.0	0.4331	0.4346	0.0015
0.5	0.3943	0.3960	0.0017
1.0	0.3065	0.3093	0.0028

mation in CCM are maximal at $\Delta = 1$, the error of m_z^{st} is only $\sim 0.9\%$. We also mention the critical behavior of m_z^{st} near $\Delta = 1$. A singularity expressed by $m_z^{\text{st}} = \sum_{n=0}^{\infty} m_n (\Delta - 1)^{n/2}$ was predicted by SWT.^{31,35,36)} However, as shown in the inset of Fig. 3(b), we find that m_z^{st} is nearly proportional to $\Delta - 1$ in the range of $1 \leq \Delta \lesssim 1.01$. This is consistent with the result from CCM.³⁸⁾ To further demonstrate the accuracy of our method, we provide a precise comparison of our large- Δ data with the result obtained by SE for $1/\Delta$. By fitting our data for $0 \leq 1/\Delta \leq 0.05$ with $2m_z^{\text{st}} = 1 + m_2/\Delta^2 + m_4/\Delta^4 + m_6/\Delta^6$, we obtain $m_2 = -0.222222225$, $m_4 = -0.0355542736$, and $m_6 = -0.0189663810$. These coefficients agree almost perfectly to the SE results: $m_2 = -2/9 = -0.222222\dots$, $m_4 = -8/255 = -0.035555\dots$, and $m_6 = -0.01894258$.^{30-33,35)}

Similarly, the magnitude of staggered magnetization in the XY phase ($-1 < \Delta < 1$) can be obtained. Since the magnetization is parallel to some arbitrary direction in the xy -plane, we here measure m_x^{st} with two pinned spins $\langle S_L^x \rangle = 1/2$ and $\langle S_{L^2-L+1}^x \rangle = -1/2$. In this case, the DMRG calculations are a little more difficult than the above estimations of m_z^{st} because S_z^{tot} is no longer conserved. Still, as shown below, sufficient data points to perform a reliable finite-size scaling analysis are available. Fig. 4(a) shows the finite-size scaling analysis of m_x^{st} for various Δ values in the XY phase, where open chains with length up to $N = L^2 = 144$ sites are used. As expected, the size-dependence of m_x^{st} becomes smaller with approaching the classical limit ($\Delta = -1$) from the isotropic point ($\Delta = 1$). In Fig. 4(b) the extrapolated values of m_x^{st} are plotted as a function of Δ . For comparison, the results from CCM³⁸⁾ are also shown. We see that m_x^{st} increases smoothly with decreasing Δ and approaches $1/2$ for $\Delta \rightarrow -1$. This confirms that the quan-

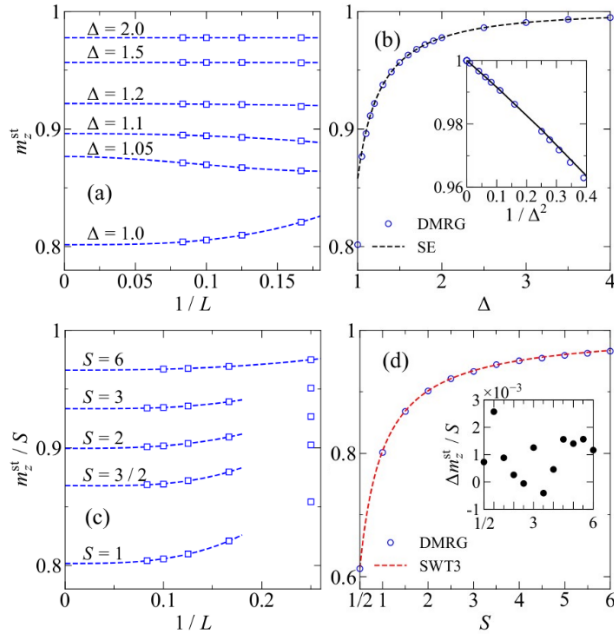


Fig. 5. (Color online) (a) Finite-size scaling analysis of m_z^{st} and (b) extrapolated values of m_z^{st} as a function of Δ for $S = 1$ and $\Delta \geq 1$. Inset: m_z^{st} vs. $1/\Delta^2$ in the large Δ region. The dashed line shows the SE result.^{34,35} (c) Finite-size scaling analysis of m_z^{st} and (d) extrapolated values of m_z^{st} as a function of S at $\Delta = 1$. The SWT results^{27–29} are shown by the red line. Inset: Difference between our DMRG and SWT results.^{27–29}

tum fluctuations of this system are strongest at $\Delta = 1$. The agreement with CCM results looks overall good. In addition, the values of m_x^{st} are compared for some Δ values in Table II. The DMRG values are only slightly smaller than the CCM ones for each Δ . This may be because that DMRG can incorporate more quantum fluctuations compared to CCM. Furthermore, we can find that our estimation of $m_x^{\text{st}} = 0.4331$ at the XY point ($\Delta = 0$) reasonably agrees to the previous estimations: $m_x^{\text{st}} = 0.43548$ by SE³⁷) and $m_x^{\text{st}} = 0.437$ by QMC.²⁵)

So far, We have verified the efficiency of our proposed method for $S = 1/2$. In practice, there is no difficulty involved in finite-size scaling of m_α^{st} ($\alpha = x, z$), so that the extrapolated values to the thermodynamic limit are quite accurate in the whole Δ region as far as has been compared to the previous studies. We then apply our method to estimate m_z^{st} for the high- S cases from $S = 1$ to $S = 6$, which is a challenging problem for numerical calculations.

Let us start with the case of $S = 1$. It is known that our system for $S \geq 1$ exhibits an Néel order for $\Delta \geq -1$.^{39,47}) As in the case of $S = 1/2$, we can calculate m_z^{st} for $\Delta \geq 1$. Finite-size scaling analyses of m_z^{st} are performed in Fig. 5(a). The extrapolated values of m_z^{st} are plotted as a function of Δ in Fig. 5(b). We obtain $m_z^{\text{st}} = 0.8017$ at $\Delta = 1$ in the thermodynamic limit. This value is in good agreement with $m_z^{\text{st}} = 0.802$ obtained by iPEPS.⁴⁸) The SE results^{34,35}) are also shown for comparison. By fitting our data for $0 \leq 1/\Delta \leq 0.03$ with $m_z^{\text{st}} = 1 + m_2/\Delta^2 + m_4/\Delta^4 + m_6/\Delta^6$, we obtain $m_2 = -0.081632653$, $m_4 = -0.026959397$, and $m_6 = -0.013867377$. These values are in good agreement with those from SE: $m_2 = -4/49 = -0.081632653 \dots$, $m_4 = -0.026959099$, and $m_6 = -0.0136997515$.^{34,35})

We next study the cases of $S > 1$. Fig. 5(c) shows the finite-

size scaling analysis of m_z^{st} for $S \geq 1$, where open chains with length up to $N = L^2 = 144$ sites are studied. As expected from the fact that the effect of quantum fluctuations is weaker for larger S , the size-dependence of m_z^{st} becomes smaller with increasing S . However, the scaling analysis can be easily done even for the smallest- S , i.e., $S = 1$ case. In Fig. 5(d) the extrapolated values of m_z^{st}/S are plotted as a function of S . We can clearly see a smooth convergence as $m_z^{\text{st}}/S \rightarrow 1$ with approaching the classical limit ($S = \infty$). The S -dependence of m_z^{st}/S has been estimated by SWT. The result up to third order is $m_z^{\text{st}}/S = 1 - 0.1966019S^{-1} + 0.000875S^{-3} + O(S^{-4})$.^{27–29}) This expression may be expected to work well for a wide range of S because the coefficients of higher order terms than $1/S$ are very small. Actually, as shown in the inset of Fig. 5(d), the difference for each S value between our results and the SWT estimations is always smaller than $\Delta m_z^{\text{st}}/S = 3 \times 10^{-3}$. By fitting our data points from $S = 1/2$ to $S = 6$ with $m_z^{\text{st}}/S = 1 + m_1S^{-1} + m_3S^{-3}$, we obtain $m_1 = -0.19895398$ and $m_3 = 0.00136057$. These values are reasonably close to those by SWT. Therefore, we confirm that our method is applicable to the high- S Heisenberg systems at least up to $S = 6$. We can also numerically confirm the absence of Haldane-like state with spin-singlet pairs on every bonds at $S = 2$.^{39,47})

In conclusion, we proposed an efficient method to obtain a local order parameter for 2D systems by DMRG using SBC. We demonstrated the validity of our method by calculating staggered magnetization of the $S = 1/2$ XXZ square-lattice Heisenberg model for the whole range of exchange anisotropy. As further application, we extended our method to the higher spin cases ($1 \leq S \leq 6$). Although we investigated an order parameter with $\mathbf{k} = (\pi, \pi)$ in this paper, ordered state with the other \mathbf{k} vectors can be considered by modifying the application of SBC.⁴⁴) Other examples of such SBC usage are given in the Supplemental Material.⁴³) We also note that a similar procedure using the projected 1D chain with periodic boundary conditions was suggested in our previous study.⁴⁵) However, the present method is much more practical because larger clusters can be studied than the previous method. In order to further clarify the advantages of SBC in DMRG simulation, finite-size scaling analysis for various boundary conditions is discussed in the Supplemental Material.⁴³)

Acknowledgment We thank Ulrike Nitzsche for technical support. This work was supported by the SFB 1143 of the Deutsche Forschungsgemeinschaft and by Grants-in-Aid for Scientific Research from JSPS (Projects No. JP20H01849, No. JP20K03769, and No. JP21J20604). M. K. acknowledges support from the JSPS Research Fellowship for Young Scientists.

- 1) W. Heisenberg, Z. Phys. **49**, 619 (1928).
- 2) M.E. Lines, Phys. Rev. **131**, 546 (1963).
- 3) N. Achiwa, J. Phys. Soc. Jpn. **27**, 561 (1969).
- 4) J.M. Kosterlitz and D.J. Thouless, J. Phys. C: Solid State Phys. **6**, 1181 (1973).
- 5) D. Opherden, M.S.J. Tepaske, F. Bärtl, M. Weber, M.M. Turnbull, T. Lancaster, S.J. Blundell, M. Baenitz, J. Wosnitzer, C.P. Landee, R. Moessner, D.J. Luitz, H. Kühne, arXiv:2209.11085.
- 6) Y. Wu, J. Xi, T. Xiao, J. Ferrando-Soria, Z. Ouyang, Z. Wang, S. Luo, X. Liu, and E. Pardo, Inorg. Chem. Front. **8**, 5158 (2021).
- 7) E.B. Sonin, Advances in Physics **59**, 181 (2010).
- 8) T.-H. Jang, S.-H. Do, M. Lee, H. Wu, C.M. Brown, A.D. Christianson, S.-W. Cheong, and J.-H. Park, Phys. Rev. B **104**, 214434 (2021).
- 9) S.-H. Do, H. Zhang, D.A. Dahlbom, T.J. Williams, V.O. Garlea,

- T. Hong, T.-H. Jang, S.-W. Cheong, J.-H. Park, K. Barros, C.D. Batista, and A.D. Christianson, arXiv:2205.11770
- 10) M. Lee, R. Schoenemann, H. Zhang, D. Dahlbom, T.-H. Jang, S.-H. Do, A.D. Christianson, S.-W. Cheong, J.-H. Park, E. Brosha, M. Jaime, K. Barros, C.D. Batista, and V.S. Zapf, arXiv:2210.14323
 - 11) T. Vasilchikova, V. Nalbandyan, I. Shukaev, H.-J. Koo, M.-H. Whangbo, A. Lozitskiy, A. Bogaychuk, V. Kuzmin, M. Tagirov, E. Vavilova, A. Vasiliev, and E. Zvereva, Phys. Rev. B **101**, 054435 (2020).
 - 12) M.D. Kuchugura, A.I. Kurbakov, E.A. Zvereva, T.M. Vasilchikova, G.V. Raganyan, A.N. Vasiliev, V.A. Barchukf, and V.B. Nalbandyan, Dalton Trans. **48**, 17070 (2019).
 - 13) M. Baenitz, M.M. Piva, S.Luther, J. Sichelschmidt, K.M. Ranjith, H. Dawczak-Dębicki, M.O. Ajeesh, S.-J. Kim, G. Siemann, C. Bigi, P. Manuel, D. Khalyavin, D.A. Sokolov, P. Mokhtari, H. Zhang, H. Yasuoka, P.D.C. King, G. Vinai, V. Polewczyk, P. Torelli, J. Wosnitza, U. Burkhardt, B. Schmidt, H. Rosner, S. Wirth, H. Kühne, M. Nicklas, and M. Schmidt, Phys. Rev. B **104**, 134410 (2021).
 - 14) J. Liu, B. Liu, L. Yuan, B. Li, L. Xie, X. Chen, H. Zhang, D. Xu, W. Tong, J. Wang, and Y. Li, New J. Phys. **23**, 033040 (2021).
 - 15) R. Rawl, L. Ge, Z. Lu, Z. Evenson, C.R.D. Cruz, Q. Huang, M. Lee, E.S. Choi, M. Mourigal, H.D. Zhou, and J. Ma, Phys. Rev. Materials **3**, 054412 (2019).
 - 16) H.K. Yoshida, M. Matsuda, M.B. Stone, C.R. dela Cruz, T. Furubayashi, M. Onoda, E. Takayama-Muromachi, and M. Isobe, Phys. Rev. Research **2**, 043211 (2020).
 - 17) C. Kim, J. Jeong, P. Park, T. Masuda, S. Asai, S. Itoh, H.-S. Kim, A. Wildes, and J.-G. Park, Phys. Rev. B **102**, 184429 (2020).
 - 18) M. Goto, H. Ueda, C. Michioka, A. Matsuo, K. Kindo, K. Sugawara, S. Kobayashi, N. Katayama, H. Sawa, and K. Yoshimura, Phys. Rev. B **97**, 224421 (2018).
 - 19) E. Kermarec, R. Kumar, G. Bernard, R. Hénaff, P. Mendels, F. Bert, P.L. Paulose, B.K. Hazra, and B. Koteswararao, Phys. Rev. Lett. **127**, 157202 (2021).
 - 20) A.M. Ferrenti, V. Meschke, S. Ghosh, J. Davis, N. Drichko, E.S. Toberer, T.M. McQueen, J. Solid State Chem. **317**, 123620 (2022).
 - 21) R. Sano, Y. Kato, and Y. Motome, Phys. Rev. B **97**, 014408 (2018).
 - 22) I. Lee, F.G. Utermohlen, D. Weber, K. Hwang, C. Zhang, J. van Tol, J.E. Goldberger, N. Trivedi, and P.C. Hammel, Phys. Rev. Lett. **124**, 017201 (2020).
 - 23) C. Xu, J. Feng, M. Kawamura, Y. Yamaji, Y. Nahas, S. Prokhorenko, Y. Qi, H. Xiang, and L. Bellaiche, Phys. Rev. Lett. **124**, 087205 (2020).
 - 24) S.R. White and A.L. Chernyshev, Phys. Rev. Lett. **99**, 127004 (2007).
 - 25) A.W. Sandvik and C.J. Hamer, Phys. Rev. B **60**, 6588 (1999).
 - 26) A.W. Sandvik and H.G. Evertz, Phys. Rev. B **82**, 024407 (2010).
 - 27) C.J. Hamer, Z. Weihong, and P. Arndt, Phys. Rev. B **46**, 6276 (1992).
 - 28) J.-i. Igarashi, Phys. Rev. B **46**, 10763 (1992).
 - 29) C.M. Canali and M. Wallin, Phys. Rev. B **48**, 3264 (1993).
 - 30) H.L. Davis, Phys. Rev. **120**, 789 (1960).
 - 31) D.A. Huse, Phys. Rev. B **37**, 2380 (1988).
 - 32) M. Parrinello and T. Arai, Phys. Rev. B **10**, 265 (1974).
 - 33) R.R.P. Singh, Phys. Rev. B **39**, 9760 (1989).
 - 34) R.R.P. Singh, Phys. Rev. B **41**, 4873 (1990).
 - 35) Z. Weihong, J. Oitmaa, and C.J. Hamer, Phys. Rev. B **43**, 8321 (1991).
 - 36) Z. Weihong, J. Oitmaa, and C.J. Hamer, Phys. Rev. B **44**, 11869 (1991).
 - 37) C.J. Hamer, J. Oitmaa, and Z. Weihong, Phys. Rev. B **43**, 10789 (1991).
 - 38) R.F. Bishop, P.H.Y. Li, R. Zinke, R. Darradi, J. Richter, D.J.J. Farnell, and J. Schulenburg, J. Magn. Magn. Mater. **428**, 178 (2017).
 - 39) K. Kubo and T. Kishi, Phys. Rev. Lett. **61**, 2585 (1988).
 - 40) V.S. Viswanath, S. Zhang, J. Stolze, and G. Müller, Phys. Rev. B **49**, 9702 (1994).
 - 41) S. Yunoki, Phys. Rev. B **65**, 092402 (2002).
 - 42) B. Braiori-Orrs, M. Weyrauch, and M.V. Rakov, Ukrainian Journal of Physics **61**, 613 (2019).
 - 43) (Supplemental material) Exact wavefunctions of the ground state at $\Delta = -1$, detailed data on the accuracy of our DMRG calculations as well as the advantages of SBC in DMRG against various boundary conditions are provided online.
 - 44) M. Nakamura, S. Masuda, and S. Nishimoto, Phys. Rev. B **104**, L121114 (2021).
 - 45) M. Kadosawa, M. Nakamura, Y. Ohta, and S. Nishimoto, arXiv:2205.15775 (2022).
 - 46) S.R. White, Phys. Rev. Lett. **69**, 2863 (1992).
 - 47) Y. Ozeki, H. Nishimori, and Y. Tomita, J. Phys. Soc. Jpn. **58**, 82 (1989).
 - 48) I. Niesen and P. Corboz, Phys. Rev. B **95**, 180404(R) (2017).

Supplemental Material for “Study of Staggered Magnetization in the Spin- S Square-Lattice Heisenberg Model Using Spiral Boundary Conditions”

Masahiro Kadosawa¹, Masaaki Nakamura², Yukinori Ohta¹, and Satoshi Nishimoto^{3,4}

¹ *Department of Physics, Chiba University, Chiba 263-8522, Japan*

² *Department of Physics, Ehime University, Ehime 790-8577, Japan*

³ *Department of Physics, Technical University Dresden, 01069 Dresden, Germany*

⁴ *Institute for Theoretical Solid State Physics, IFW Dresden, 01069 Dresden, Germany*

(Dated: January 2, 2023)

I. EXACT GROUND STATE AT $\Delta = -1$

As mentioned in the main text, the system (1) exhibits a first-order transition between easy-plane Néel (XY) and ferromagnetic (FM) phases at $\Delta = -1$. At this critical point, the ground state is two-fold degenerate with energy $E_0 = -2NS^2$. One of them for $\Delta < -1$ side is a simple FM state expressed as

$$|\Psi_0(\text{FM})\rangle = \frac{1}{\sqrt{2}}(|\uparrow\rangle + |\downarrow\rangle), \quad (\text{S1})$$

where $|\uparrow\rangle$ and $|\downarrow\rangle$ denote fully-polarized states towards the z and $-z$ directions, respectively. On the other hand, for $\Delta > -1$ side the spins are antiferromagnetically aligned on the xy -plane. The direction of magnetization is arbitrary. This state is expressed as

$$|\Psi_0(\text{XY})\rangle = \sum_m \lambda_m |\psi_m\rangle, \quad (\text{S2})$$

where $|\psi_m\rangle$ are bases restricted to $S_{\text{tot}}^z = \sum_{i=1}^{L^2} \langle S_i^z \rangle = 0$ subspace, and m is summed over all possible combinations of spin configurations. Two coefficients have a relation $\lambda_m = (-1)^n \lambda'_m$ if a basis $|\psi_m\rangle$ is obtained by n exchange processes from another basis $|\psi'_m\rangle$. In the following subsections, we show this state specifically for the cases of $S = 1/2$ and $S = 1$.

A. $S = 1/2$

In this case, a state for each site is represented by either spin-up ($|\uparrow\rangle$) or spin-down ($|\downarrow\rangle$) states. Because of $S_{\text{tot}}^z = 0$, an N -site lattice system contains $\frac{N}{2}$ up and $\frac{N}{2}$ down spins. Since there are only two states are allowed in each site, the coefficient $|\lambda_m|$ takes a value of either $\frac{1}{\sqrt{\mathcal{P}}}$ or $-\frac{1}{\sqrt{\mathcal{P}}}$. The total number of spin configurations is given by $\mathcal{P} = \frac{N!}{(N/2)!(N/2)!}$.

B. $S = 1$

In this case, a state for each site is any one of spin-up ($|\uparrow\rangle$), spin-down ($|\downarrow\rangle$), and spin-0 ($|0\rangle$) states. Because of $S_{\text{tot}}^z = 0$, the numbers of spin-up and spin-down sites should be the same. By setting them to be $r/2$, the number of spin-0 sites is $N-r$ for an N -site lattice system. The absolute value of the coefficient depends on r like $|\lambda_m| = 2^{N-2r} |a|$. The value of a is determined by a condition

$$|a|^2 \sum_{r=0}^{N/2} \binom{N}{r} C_{2r} C_r 2^{N-2r} = 1. \quad (\text{S3})$$

II. COMPARISON WITH SERIES EXPANSION OF $1/\Delta$ FOR $S = 1/2$

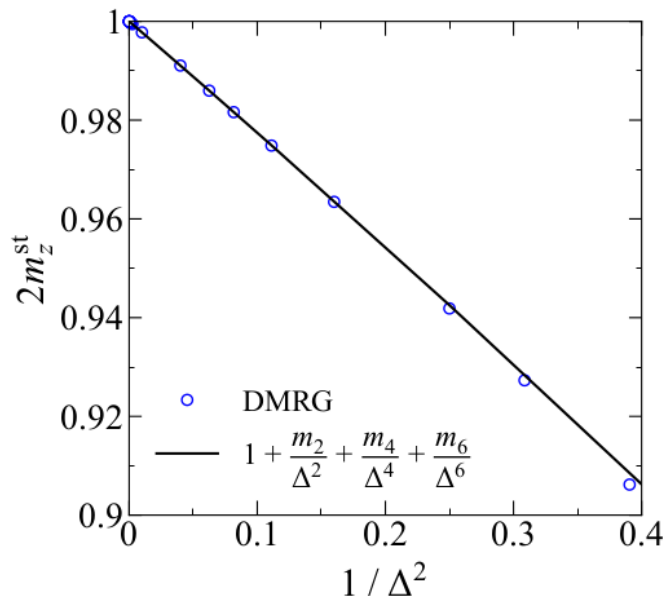


FIG. S1: DMRG results for magnitude of the staggered magnetization of the $S = 1/2$ square-lattice Heisenberg model as a function of $1/\Delta^2$. The solid line shows fitting by a polynomial function $2m_z^{\text{st}} = 1 + m_2/\Delta^2 + m_4/\Delta^4 + m_6/\Delta^6$.

In Fig. S1 the DMRG results for magnitude of the staggered magnetization of the $S = 1/2$ square-lattice Heisenberg model are plotted as a function of $1/\Delta^2$. Our data in the large- Δ region ($0 \leq 1/\Delta \leq 0.05$) can be fitted by $2m_z^{\text{st}} = 1 + m_2/\Delta^2 + m_4/\Delta^4 + m_6/\Delta^6$ with $m_2 = -0.222222225$, $m_4 = -0.0355542736$, and $m_6 = -0.0189663810$. This agrees well with the series expansions $2m_z^{\text{st}} = 1 - (2/9)/\Delta^2 - (8/225)/\Delta^4 - 0.01894258/\Delta^6 + \mathcal{O}(1/\Delta^8)$ [$2/9 = 0.22222222 \dots$, $8/225 = 0.0355555 \dots$] [1].

[1] Z. Weihong, J. Oitmaa, and C.J. Hamer, Phys. Rev. B **43**, 8321 (1991).

III. COMPARISON WITH SERIES EXPANSION OF $1/S$

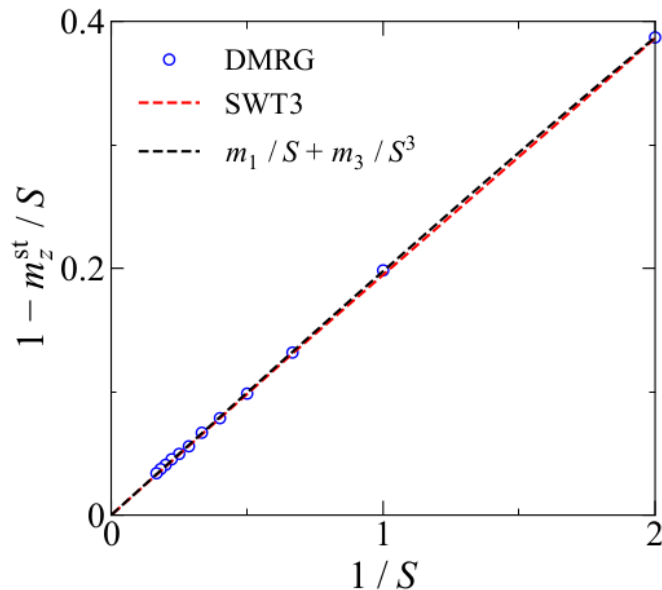


FIG. S2: DMRG results for magnitude of the staggered magnetization of the square-lattice isotropic Heisenberg model as a function of $1/S$. The red and black dotted lines are SWT results and fitting by a polynomial function $m_z^{\text{st}}/S = 1 + m_1 S^{-1} + m_3 S^{-3}$, respectively.

The S -dependence of m_z^{st}/S has been estimated by spin wave theory (SWT). The result up to third order is $m_z^{\text{st}}/S = 1 - 0.1966019S^{-1} + 0.00087S^{-3} + O(S^{-4})$ [1–3]. This expression may be expected to work well for a wide range of S because the coefficients of higher order terms than $1/S$ are very small. As shown in Fig. S3, we can see a good agreement between our results and SWT. By fitting our data points from $S = 1/2$ to $S = 6$ with $m_z^{\text{st}}/S = 1 + m_1 S^{-1} + m_3 S^{-3}$, we obtain $m_1 = -0.19895398$ and $m_3 = 0.00136057$. These values are reasonably close to those by SWT.

-
- [1] C.J. Hamer, Z. Weihong, and P. Arndt, Phys. Rev. B **46**, 6276 (1992).
 - [2] J.-i. Igarashi, Phys. Rev. B **46**, 10763 (1992).
 - [3] C.M. Canali and M. Wallin, Phys. Rev. B **48**, 3264 (1993).

IV. FLEXIBILITY OF SPIRAL BOUNDARY CONDITIONS

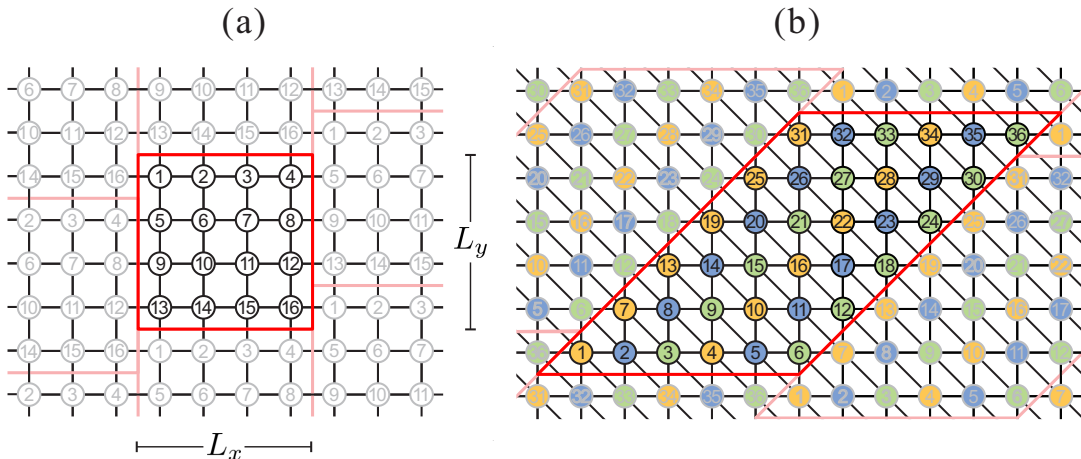


FIG. S3: (a) 2D square-lattice cluster where a region framed by red line is the original cluster. This application of SBC is consistent with an ordered state with modulation of $\mathbf{k} = (\pi, 0)$. (b) 2D triangular-lattice cluster where a region framed by red line is the original cluster. This application of SBC is consistent with an ordered state with modulation of $\mathbf{k} = (2\pi/3, 2\pi/3)$. The sites belonging to different sublattices are color-coded.

As noted in the main text, the ordering vector can be controlled by modifying the application way of SBC [1]. The way used for 2D square lattice in the main text is appropriate to study a state with modulation of $\mathbf{k} = (\pi, \pi)$, like a Néel state. However, if we study a state with modulation of $\mathbf{k} = (\pi, 0)$, it is more convenient to use another application way of SBC. It is shown in Fig. S3(a). In this way, the original 2D square-lattice cluster with $L_x \times L_y$ sites can be exactly mapped onto a 1D chain with nearest- and L_x -th neighbor hopping integrals, where the translation symmetry is also preserved. The Hamiltonian is written as

$$\mathcal{H}_{0,\text{sq}} = -t \sum_{\sigma} \sum_{i=1}^{L_x L_y} (c_{i,\sigma}^{\dagger} c_{i+1,\sigma} + c_{i,\sigma}^{\dagger} c_{i+L_x,\sigma} + \text{H.c.}), \quad (\text{S4})$$

and its Fourier transform leads to

$$\mathcal{H}_{\text{sq},K} = -2t \sum_{K,\sigma} (\cos K + \cos L_x K) c_{K,\sigma}^{\dagger} c_{K,\sigma}, \quad (\text{S5})$$

where $n = n_x + L_x n_y = 0, 1, \dots, L_x L_y - 1$). It is interesting that both $\mathbf{k} = (\pi, \pi)$ in Fig. 1(a) of the main text and $\mathbf{k} = (\pi, 0)$ in Fig. S3(a) are represented by a $k = \pi$ modulation in the projected 1D chain.

As another example, let us consider a state with modulation of $\mathbf{k} = (2\pi/3, 2\pi/3)$. This corresponds to a 120° structure in the triangular-lattice Heisenberg model. Similarly, this state can be represented by 1D chain with translation symmetry, as shown in Fig. S3(b). For a cluster with $L_x \times L_y$ sites, the 2D system can be exactly mapped onto a 1D chain with nearest-, $(L_x - 2)$ -th, and $(L_x - 1)$ -th neighbor bonds.

As shown above, the modulation of cluster can be flexibly controlled. In the case of incommensurate order, it would be able to make a convergence of physical quantity to the thermodynamic limit faster by realizing a possibly closest modulation to the incommensurate vector.

[1] M. Nakamura, S. Masuda, and S. Nishimoto, Phys. Rev. B **104**, L121114 (2021).

V. CORRELATION FUNCTIONS FOR VARIOUS BOUNDARY CONDITIONS

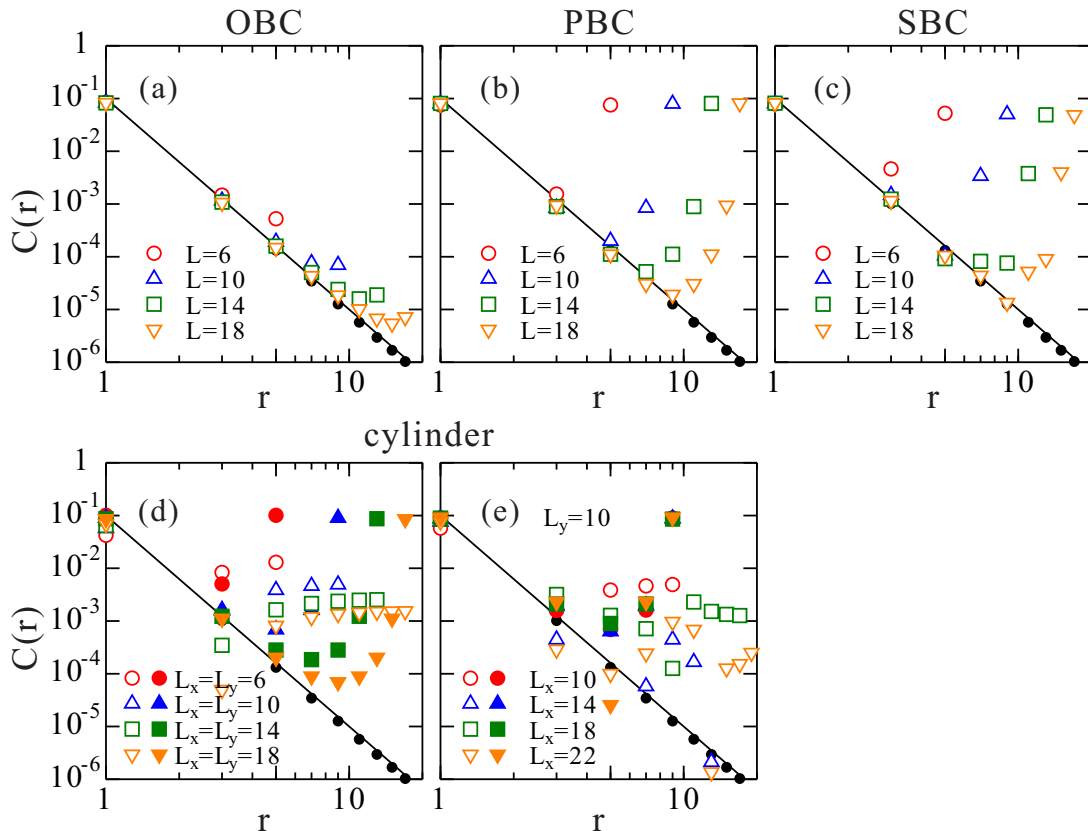


FIG. S4: Density-density correlation functions $C(r)$ for non-interacting fermions on a 2D square lattice at half filling as a function of distance r along bond direction, namely, $(1,0)$ or $(0,1)$, with (a) OBC, (b) PBC, (c) SBC, and (d,e) cylinder. For cylinder, the values for both $(1,0)$ and $(0,1)$ directions are shown. As a reference data, the result for very large system with 100×100 OBC cluster is plotted by black dots. As expected, it decays like $C(r) \propto 1/r^4$ (black line).

It is interesting to see how correlation functions are affected by boundary conditions. To investigate their long-range behavior, we consider the density-density correlation functions $C(r) = 1 - \langle n_i n_{i+r} \rangle$ of non-interacting fermions on a 2D square lattice because they can be exactly obtained. In Fig. S4 we plot $C(r) = 1 - \langle n_i n_{i+r} \rangle$ as a function of distance r along bond direction, namely, $(1,0)$ or $(0,1)$, at half filling for various boundary conditions. We find that OBC, PBC, and SBC can provide equally good results: For example, the data points up to $r \sim 9$ are almost on the analytical line $C(r) \propto 1/r^4$ for the systems with $L = 18$. On the other hand, the result with cylindrical cluster is obviously worst, namely, the deviation from $C(r) \propto 1/r^4$ is largest. As is well known [1], the result seems to be improved by increasing the system size with keeping the ratio between system length and circumference. Nevertheless, the behavior $C(r) \propto 1/r^4$ can be confirmed only up to $r \sim 5$ in the case of $L_x = L_y = 18$ [see Fig. S4(d)]. It is because that cylindrical boundary conditions impose a kind of spatial anisotropy on the original isotropic 2D square-lattice cluster. Furthermore, surprisingly, the result cannot be improved by increasing the system length if the circumference is kept [Fig. S4(e)].

As discussed above, we may choose either OBC or SBC when correlation functions for 2D system are studied. However, a 2D system under OBC can be easily disturbed by Friedel oscillations once it is doped or any interaction is switched on. Therefore, SBC could be a first choice for DMRG study of correlation functions for 2D systems.

[1] A.W. Sandvik, Phys. Rev. B **85**, 134407 (2012).

VI. SIZE SCALING OF GROUND-STATE ENERGY FOR VARIOUS BOUNDARY CONDITIONS

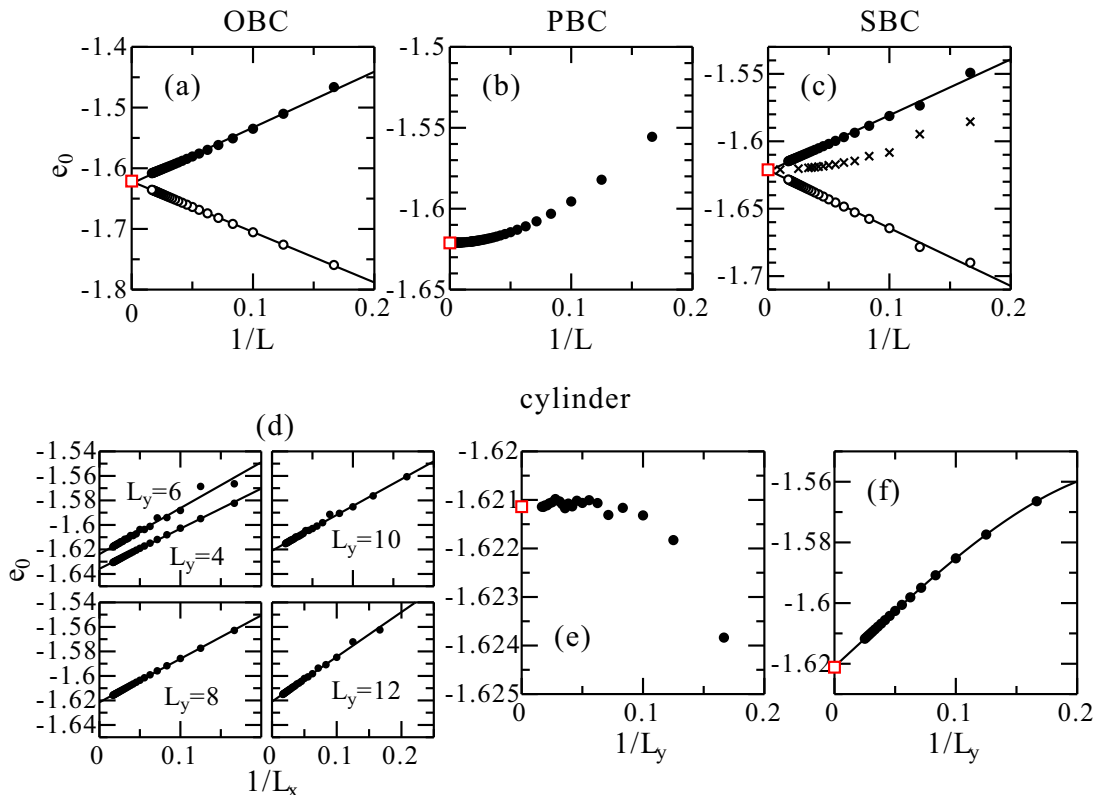


FIG. S5: Finite-size-scaling analysis of the ground-state energy for non-interacting fermions on a 2D square lattice at half filling with (a) OBC, (b) PBC, (c) SBC, and (d-f) cylinder. The exact ground-state energy in the thermodynamic limit, $e_0 = -16/\pi^2$, is denoted by red square. The solid and open circles denote the ground state energy per site and per two bonds, respectively. For cylinder, scaling analyses along system length L_x for given circumferences L_y are performed in (d), and then scaling analysis along circumference direction is performed in (e), where the extrapolated values obtained in (d) are used. Also, scaling analysis with keeping $L_x = L_y$ is performed in (f).

We here look into finite-size-scaling behavior of the ground-state energy for each of boundary conditions. In Fig. S5 we perform finite-size-scaling analyses of the ground-state energy for non-interacting fermions on a 2D square lattice at half filling with various boundary conditions. The scaling behavior for OBC is straightforward [Fig. S5(a)], which is similar to that for the case of 1D projected open chain under SBC [Fig. S5(c)]. On the other hand, the ground-state energy approaches to its thermodynamic-limit value as $1/L^2$ for PBC. If we use DMRG, the ground-state energies can be calculated only for $L \lesssim 10$ with 2D periodic clusters. Thus, the finite-size-scaling analysis of the ground-state energy would be difficult for PBC.

When we use cylinder, finite-size-scaling analysis must be performed along two orientations, e.g., x - and y -directions. First, the scaling analyses along system length L_x for given circumferences L_y are performed to obtain the $L_x \rightarrow \infty$ values of the ground-state energy for each L_y [Fig. S5(d)]. Next, with using the obtained $L_x \rightarrow \infty$ values further scaling analysis along circumference direction L_y is performed [Fig. S5(e)]. Similarly to the case of PBC, the scaling behavior looks like $e_0 = -16/\pi^2 + \alpha/L_y^\beta$ ($\alpha < 0$, $\beta > 2$). Therefore, accurate estimation of the ground-state energy for 2D itinerant systems using DMRG with cylindrical clusters may be not very practical, considering that there would be some uncertainty in the extrapolation to $L_x \rightarrow \infty$ and the extrapolated values can be obtained only for $L_y \lesssim 10$. We also perform a scaling analysis with keeping $L_x = L_y$ in Fig. S5(f). The scaling behavior looks simple but deviates from a linear function like for OBC and open chain under SBC.

For the above reason, OBC or SBC would be a best choice for estimating the ground-state energy of 2D systems in the thermodynamic limit.

VII. CONVERGENCE CHECK OF DMRG CALCULATIONS

TABLE I: Discarded weight w_d and the ground-state energy $E_0(m)$ of the half-filled square-lattice Hubbard model at $U/t = 8$ as functions of system size $L \times L$ and the number of density-matrix eigenstates kept in the renormalization m , where SBC are applied. The ground-state energy at $m \rightarrow \infty$ was obtained by a linear fit of $E_0(m)$ vs. w_d .

$L = 6$				$L = 8$			
m	w_d	$E_0(m)$	$E_0(m) - E_0(\infty)$	m	w_d	$E_0(m)$	$E_0(m) - E_0(\infty)$
2000	3.432e-06	-17.79364790	0.01227902	2000	1.286e-05	-31.76311291	0.26322934
4000	7.856e-07	-17.80326286	0.00266406	4000	8.420e-06	-31.87302879	0.15331346
6000	3.052e-07	-17.80489349	0.00103344	6000	5.681e-06	-31.91448613	0.11185612
8000	1.516e-07	-17.80541043	0.00051649	8000	4.550e-06	-31.93686464	0.08947761
10000	8.614e-08	-17.80563244	0.00029448	10000	4.165e-06	-31.95093410	0.07540815
12000	5.332e-08	-17.80574150	0.00018542	12000	3.815e-06	-31.96253340	0.06380885
∞		-17.80592692		∞		-32.02634225	

$L = 10$				$L = 12$			
m	w_d	$E_0(m)$	$E_0(m) - E_0(\infty)$	m	w_d	$E_0(m)$	$E_0(m) - E_0(\infty)$
2000	2.119e-05	-49.50077175	1.02132882	2000	-	-	-
4000	1.379e-05	-49.84727132	0.67482925	4000	1.840e-05	-71.40452905	1.73164686
6000	1.198e-05	-49.99628942	0.52581115	6000	1.486e-05	-71.71734724	1.41882867
8000	9.848e-06	-50.09485526	0.42724531	8000	1.365e-05	-71.91712273	1.21905318
10000	7.774e-06	-50.15642914	0.36567143	10000	1.224e-05	-72.06942431	1.06675160
12000	5.854e-06	-50.19615496	0.32594561	12000	9.293e-06	-72.19219444	0.94398147
∞		-50.52210057		∞		-73.13617591	

We here check the accuracy of DMRG calculations under SBC (periodic chain). In Table I the Discarded weight w_d and the ground-state energy $E_0(m)$ of the half-filled square-lattice Hubbard model at $U/t = 8$ are shown as a function of the number of density-matrix eigenstates kept in the renormalization m for various system sizes $L \times L$. For all cases the ground-state energy at $m \rightarrow \infty$ ($w_d \rightarrow 0$) can be accurately obtained by a linear fit of $E_0(m)$ vs. w_d . We also find that the discarded weight is roughly proportional to L , i.e., $w_d \propto L$. Nevertheless, the discarded weight is still order of $\sim 10^{-5}$ even for 12×12 . This may fall into the category of an accurate DMRG calculation for 2D fermionic system.

In Table II the discarded weight in the DMRG calculation for the square-lattice Heisenberg model is compared between various boundary conditions. The discarded weight is almost comparable for OBC and cylinder, and somewhat larger for the SBC-projected periodic chain. Surprisingly, it is much smaller when the SBC-projected open chain is studied. Thus, from the viewpoint of discarded weight, OBC, SBC, and cylinder can be equally good options in DMRG calculation for 2D systems

TABLE II: Discarded weight w_d and the ground-state energy $E_0(m)$ of the square-lattice Heisenberg model as a function of the number of density-matrix eigenstates kept in the renormalization m for system sizes 6×6 ($L = 6$) and 8×8 ($L = 8$) with various boundary conditions. The ground-state energy at $m \rightarrow \infty$ was obtained by a linear fit of $E_0(m)$ vs. w_d .

OBC						
m	$L = 6$			$L = 8$		
	w_d	$E_0(m)$	$E_0(m) - E_0(\infty)$	w_d	$E_0(m)$	$E_0(m) - E_0(\infty)$
1000	1.100e-07	-21.72673267	0.00005340	8.166e-06	-39.60759545	0.01078493
2000	6.466e-09	-21.72678301	0.00000307	1.587e-06	-39.61627493	0.00210544
3000	9.883e-10	-21.72678556	0.00000051	5.714e-07	-39.61762743	0.00075294
4000	2.279e-10	-21.72678592	0.00000015	2.636e-07	-39.61803809	0.00034228
		-21.72678607			-39.61838038	

PBC						
m	$L = 6$			$L = 8$		
	w_d	$E_0(m)$	$E_0(m) - E_0(\infty)$	w_d	$E_0(m)$	$E_0(m) - E_0(\infty)$
1000	2.981e-05	-24.40302953	0.03665799	-	-	-
2000	9.188e-06	-24.42949472	0.01019281	-	-	-
3000	3.938e-06	-24.43541285	0.00427468	-	-	-
4000	1.982e-06	-24.43743236	0.00225516	-	-	-
		-24.43968752				

SBC (periodic chain)						
m	$L = 6$			$L = 8$		
	w_d	$E_0(m)$	$E_0(m) - E_0(\infty)$	w_d	$E_0(m)$	$E_0(m) - E_0(\infty)$
1000	9.130e-06	-24.45300594	0.00801971	9.025e-05	-42.79118365	0.32899812
2000	1.661e-06	-24.45965335	0.00137230	4.565e-05	-42.96307806	0.15710371
3000	5.365e-07	-24.46058729	0.00043835	2.898e-05	-43.02157949	0.09860228
4000	2.260e-07	-24.46083548	0.00019017	1.973e-05	-43.05183014	0.06835163
∞		-24.46102565			-43.12018177	

SBC (open chain)						
m	$L = 6$			$L = 8$		
	w_d	$E_0(m)$	$E_0(m) - E_0(\infty)$	w_d	$E_0(m)$	$E_0(m) - E_0(\infty)$
1000	1.037e-09	-23.07464567	0.00000050	9.819e-07	-41.31375095	0.00116164
2000	2.447e-11	-23.07464616	0.00000001	1.161e-07	-41.31476448	0.00014811
3000	2.351e-12	-23.07464617	$< 10^{-8}$	2.987e-08	-41.31487486	0.00003773
4000	3.837e-13	-23.07464618	$< 10^{-8}$	1.058e-08	-41.31489881	0.00001379
∞		-23.07464618			-41.31491259	

cylinder						
m	$L = 6$			$L = 8$		
	w_d	$E_0(m)$	$E_0(m) - E_0(\infty)$	w_d	$E_0(m)$	$E_0(m) - E_0(\infty)$
1000	3.349e-08	-23.09009340	0.00001678	4.299e-06	-41.34358356	0.00569929
2000	1.512e-09	-23.09010942	0.00000076	7.206e-07	-41.34831869	0.00096415
3000	2.012e-10	-23.09011008	0.00000010	2.330e-07	-41.34898086	0.00030198
4000	4.556e-11	-23.09011016	0.00000002	9.196e-08	-41.34916154	0.00012131
∞		-23.09011018			-41.34928284	

VIII. ADVANTAGES OF SPIRAL BOUNDARY CONDITIONS

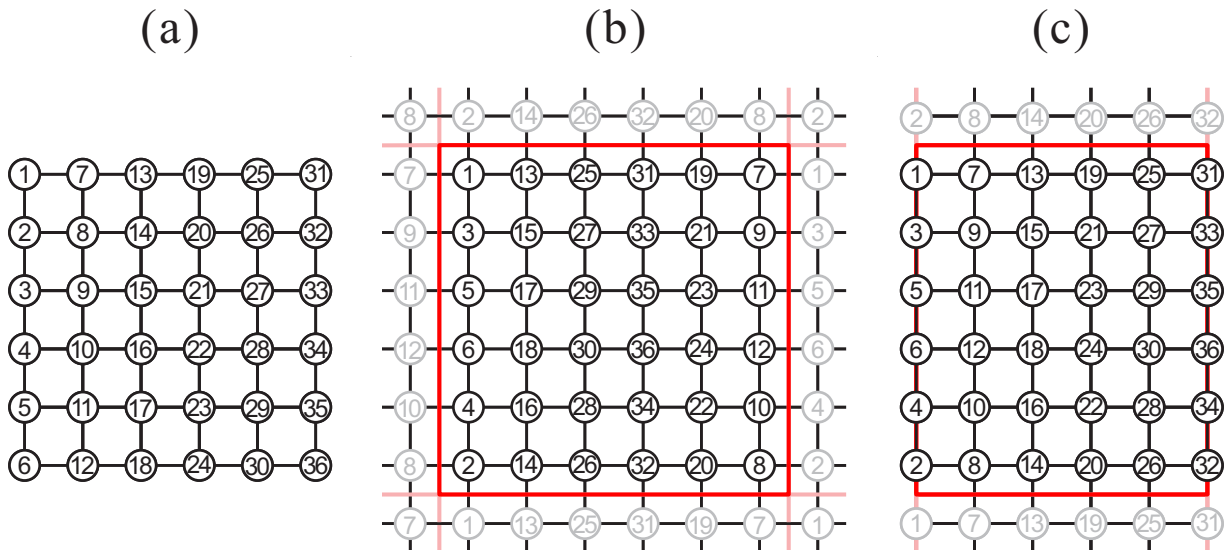


FIG. S6: 2D square-lattice 6×6 cluster with (a) OBC, (b) PBC, and (c) cylinder. In each cluster an optimal order of sites for DMRG simulation is denoted by numbers.

In DMRG simulations we have to choose a proper boundary condition for considered system and quantities. The applicability of DMRG to a lattice system can be roughly judged by the distance between two sites connected by the longest-range term in the system. The distance is denoted by d below. In general, the DMRG calculation is difficult if d is larger than ~ 10 . Let us then estimate the values of d for various boundary conditions. In Fig. S6 an optimal order of sites to give the shortest d for a 2D square-lattice cluster is illustrated for each boundary condition. When we use OBC or cylinder, d is L for a $L \times L$ cluster. This is comparable to that for SBC ($d = L - 1$ or $d = L$). However, if we use PBC, d jumps to $2L$. This is definitely ill-conditioned for DMRG treatments. For example, the system size is limited up to $L \sim 6$ in the Heisenberg model. Therefore, PBC may be firstly excluded from the choice, although it is naively thought to be a most versatile boundary condition in numerical calculations.

In fact, either OBC or cylinder is typically employed in the previous DMRG simulations. These boundary conditions are technically rather convenient for DMRG simulations because the value of d can be reduced down to L with the optimal order of sites. Nevertheless, they could often lead to some sorts of problems in the physical properties. The followings are examples of issues: With OBC, the bulk state can be significantly disturbed by Friedel oscillations, and also the properties of bulk and edge states can be completely different due to the missing outside bonds especially in doped systems. These problems could be managed by controlling open edges for a specific states, and however, it is not always successful. With cylinder, a kind of spatial anisotropy is introduced in spite of the original isotropic 2D square-lattice cluster. A most problematic point is that short loops of bonds are formed along the circumference direction. This could results in an unnatural periodicity of the wave function as well as an unexpected plaquette constraint of particles or spins. Accordingly, as shown in the previous section of Supplemental Material, the density-density correlation functions can be largely disturbed by cylindrical boundary.

With SBC, Friedel oscillations can be avoidable and no artificial short loops of bonds are created. Also, d is only L or $L - 1$. Furthermore, a SBC-projected chain with open boundary is used, the accuracy of DMRG calculation is even better than that with OBC and cylinder as shown in the previous section of Supplemental Material. Thus, SBC enables us to perform accurate DMRG calculations with skirting some sorts of finite-size effects seen in OBC and cylindrical clusters. However, we expect that SBC does not always provide better results. For example, OBC may be more appropriate to study a system exhibiting valence-bond-solid state such as plaquette/bond order; and, a cylindrical cluster may be more appropriate to study a system exhibiting magnetic/charge/bond ordered state with spatial rotation symmetry breaking.

We thus think that SBC can be a main option of the boundary conditions in DMRG calculations for the above technical and physical reasons.